

## RESEARCH LETTER

10.1029/2018GL080046

### Key Points:

- Top-of-atmosphere net radiation is weakly sensitive to large-scale atmospheric circulation over the tropical west Pacific
- As the large-scale upward motion increases, the proportion of thick-to-thin convective cloud remains nearly constant
- Convective systems in the Community Atmosphere Model version 5 contain too much physically and optically thick cloud and too little thin cloud

### Supporting Information:

- Supporting Information S1

### Correspondence to:

C. J. Wall,  
caseyw8@uw.edu

### Citation:

Wall, C. J., & Hartmann, D. L. (2018). Balanced cloud radiative effects across a range of dynamical conditions over the tropical West Pacific. *Geophysical Research Letters*, 45, 11,490–11,498. <https://doi.org/10.1029/2018GL080046>

Received 14 AUG 2018

Accepted 13 OCT 2018

Accepted article online 17 OCT 2018

Published online 29 OCT 2018

## Balanced Cloud Radiative Effects Across a Range of Dynamical Conditions Over the Tropical West Pacific

Casey J. Wall<sup>1</sup>  and Dennis L. Hartmann<sup>1</sup> 

<sup>1</sup>Department of Atmospheric Sciences, University of Washington, Seattle, WA, USA

**Abstract** Instantaneous relationships between clouds and large-scale vertical motion are used to study the impact of circulation on the near cancellation of cloud radiative effects that is observed over the tropical west Pacific Ocean. The coverage of deep-convective clouds increases with stronger upward motion, but the proportion of thick, medium, and thin anvil cloud remains nearly constant. Thus, when averaging over scales larger than individual storms, the top-of-atmosphere net radiation is only weakly sensitive to the large-scale flow. The balance in cloud radiative effects is therefore maintained across a wide range of large-scale circulations. The ability of the Community Atmosphere Model Version 5 to reproduce the observed cloud-circulation relationships is investigated. The simulated convective clouds substantially overestimate the proportion of deep and optically thick cloud and underestimate the proportion of anvil cirrus. These results demonstrate that simulating key properties of deep-convective clouds remains challenging for some state-of-the-art climate models.

**Plain Language Summary** The high-cloud systems that are found over warm tropical oceans typically contain thick, rainy clouds connected to thinner extended ice clouds. The thick clouds have a cooling effect on Earth's climate because of their ability to reflect incoming sunlight back to space, while the thin clouds have a warming effect because of their ability to trap outgoing thermal infrared radiation. These warming and cooling effects cancel one another very closely, but why they do so is unknown. In this study we use satellite data to show that the cancellation is maintained as the large-scale atmospheric circulation varies. We also show that a state-of-the-art climate model does not reproduce this behavior.

## 1. Introduction

Clouds fundamentally shape Earth's radiation budget, and future changes in cloud radiative effects are the largest single source of uncertainty in climate projections (Caldwell et al., 2016; Dufresne & Bony, 2008). Better understanding of cloud processes and better representation of clouds in climate models are therefore vital goals for climate research.

Tropical deep-convective regions are of particular interest because they contain vast quantities of high clouds. Regions of maritime convection, like the tropical western Pacific and the Indian Ocean, contain a diverse cloud population with radiative effects that range from warming to strongly cooling the climate system (Hartmann & Berry, 2017). Deep-convective regions therefore have the potential to contribute large positive or negative cloud feedbacks on future climate change. However, when averaged over the satellite record, the shortwave (SW) and longwave (LW) cloud radiative effects (CREs) of the diverse cloud population are nearly equal and opposite (Ramanathan et al., 1989). It has been argued that this balance in CRE results from a fortuitous coincidence (Kiehl, 1994); from interactions between clouds, large-scale atmospheric circulation, and sea surface temperature (SST; Hartmann et al., 2001); and from interactions between cloud radiative heating, turbulence, and cloud microphysical processes (Hartmann & Berry, 2017). These theories raise several interesting questions: If the seemingly delicate balance in CRE is not coincidental and is enforced by some process internal to the climate system, then will that process limit future cloud changes in the tropics? And if so, are climate models able to simulate this?

In this study we work toward answering these questions by investigating the extent to which large-scale circulations play a role in the CRE balance. We examine the sensitivity of clouds and the top-of-atmosphere radiation budget to variations in large-scale atmospheric circulation, both in satellite observations and in the Community Atmosphere Model Version 5 (CAM5). The data and methods are described in section 2,

results are presented in section 3, implications for the theories on the CRE balance and for climate projections are discussed in section 4, and a summary is presented in section 5.

## 2. Data and Methods

### 2.1. Observational Data

We use observations from the CERES-CloudSat-CALIPSO-MODIS data set version RelB1 (CERES Science Team, 2016; Kato et al., 2010), which includes instantaneous, footprint-level measurements from multiple satellites from the A-Train constellation (Stephens et al., 2002). CloudSat and CALIPSO retrieve the vertical structure of clouds, CERES retrieves broadband radiative fluxes, and MODIS retrieves properties of the highest clouds. Measurements are averaged over the CERES footprints, which have horizontal resolution of  $\sim 30$  km. We will focus on cloud structure retrieved by CloudSat and CALIPSO and on radiative fluxes retrieved by CERES. These are the best satellite-based estimates of these quantities that are currently available. The variables used in this study are listed in Table S1 in the supporting information.

We also use vertical pressure velocity at 500 hPa ( $\omega_{500}$ ) from the European Center for Medium-Range Weather Forecasts Reanalysis as a measure of large-scale atmospheric circulation (Dee et al., 2011; ECMWF, 2015). This data set includes instantaneous realizations of  $\omega_{500}$  every 6 hr with  $0.75^\circ \times 0.75^\circ$  horizontal resolution. The instantaneous  $\omega_{500}$  data are sensitive to the convective parameterization in the reanalysis model and hence have large uncertainties (Bretherton & Hartmann, 2009). However, we checked if these uncertainties impact the conclusions by repeating the analysis using scatterometer observations of low-level winds, which provide an independent measure of the large-scale flow (Fore et al., 2014; SeaPAC, 2018). The main conclusions are the same if  $\omega_{500}$  or divergence of the low-level winds is used as an index of large-scale circulation (see supporting information).

We analyze measurements from the tropical west Pacific ( $12^\circ\text{N}$ – $12^\circ\text{S}$ ,  $150^\circ\text{E}$ – $170^\circ\text{E}$ ) during July–August of 2006 and June–August of 2007–2010. This domain is typical of tropical regions with warm and uniform SST and enhanced deep convection, including the Indian Ocean and the broader west Pacific warm pool (Hartmann & Berry, 2017).

### 2.2. Community Atmosphere Model Version 5

We also study cloud-circulation relationships in the CAM5 (Neale et al., 2012), which is a state-of-the-art global climate model (GCM) from the Coupled Model Intercomparison Project Phase 5 (CMIP5). CAM5 uses several parameterizations to represent cloud processes, including cloud microphysics (Morrison & Gettelman, 2008), cloud macrophysics (Park et al., 2014), shallow convection (Park & Bretherton, 2009), deep convection (Zhang & McFarlane, 1995), and turbulent mixing (Bretherton & Park, 2009). The model is run with a finite volume dynamical core, with SST prescribed to observed values following the Atmosphere Model Intercomparison Project protocol (Gates, 1992), and with standard resolution of  $0.9^\circ$  latitude and  $1.25^\circ$  longitude. A period of 2 years and 5 months is used for model spin-up. The CFMIP Observation Simulator Package is run inline during the simulation (Bodas-Salcedo et al., 2011). Instantaneous output is generated every 6 hr, and the years 2003–2006 are analyzed.

### 2.3. Methods

To compute cloud-circulation relationships, the  $\omega_{500}$  values are linearly interpolated to the time and location of each CERES footprint. Cloud data are then composited based on  $\omega_{500}$ , and the average of each bin is computed. The standard error of the mean (SE) is used to estimate uncertainty:

$$SE = \sigma / \sqrt{N}$$

Here  $\sigma$  is the sample standard deviation and  $N$  is the effective degrees of freedom. The value  $N$  is determined using the CloudSat vertical feature mask, which classifies clouds into eight types based on cloud vertical structure (Sassen & Wang, 2008). In a string of consecutive satellite footprints, two neighboring footprints are considered independent only if their predominant cloud types are different. The 95% confidence interval for the mean is  $\pm 1.96$  SE.

Sampling limitations are an additional source of uncertainty. Since the A-Train follows a Sun-synchronous orbit, and since CloudSat and CALIPSO house nadir-staring instruments, all measurements in the observational data set were made around 1:30 p.m. and 1:30 a.m. local time. For SW CRE, averaging measurements from these times is a poor approximation of the daily-mean value. To mitigate this issue, we use the afternoon measurements and compute SW CRE using daily-mean insolation:

$$\text{SW CRE} = (\alpha_{\text{clear sky}} - \alpha_{\text{all sky}}) \overline{\text{SW}}_{\downarrow} \quad (1)$$

where  $\alpha$  is albedo and  $\overline{\text{SW}}_{\downarrow}$  is the daily-mean insolation at the measurement location. This approximation will hold if the proportion of optically thick, medium, and thin anvil coverage is similar for storms that initiate at different hours of the day. We checked the validity of this approximation using 3 months of hourly data from the CERES SYN1deg-1Hour data set, which includes the full diurnal cycle (CERES Science Team, 2017a, 2017b). The average CRE over the 3-month period estimated from equation (1) agrees with the true average CRE to within  $2 \text{ Wm}^{-2}$ , and the approximation retains the relationships between CRE and large-scale vertical motion (Figure S2 in the supporting information).

Model data are treated as similarly as possible to the observations. This includes using satellite simulators to facilitate a direct model-to-observation comparison. For every time step and model column, the satellite simulators generate 150 “subcolumns” that represent the subgrid-scale variability of clouds, and then use the subcolumns to simulate footprint retrievals from the A-Train satellites (Chepfer et al., 2008; Haynes et al., 2007; Klein & Jakob, 1999; Pincus et al., 2012). The statistics of the simulated retrievals can be compared to real data if both are aggregated in a consistent way. Here we aggregate the simulated and real retrievals by compositing based on  $\omega_{500}$ . Since the CAM5 and reanalysis data sets have comparable resolution, it is fair to compare observations and model output in this way.

Care is also taken to account for the sampling limitations of the satellites. Instantaneous model output is generated every 6 hr, and for each model grid point, the hour closest to the time of the A-Train afternoon overpass is selected for analysis. SW CRE is calculated using these data and equation (1), as in the observations.

One major difference between the observations and CAM5 is the treatment of cloud detection by CloudSat. The observational data set includes cloud fraction retrieved by CloudSat and CALIPSO, while the CloudSat simulator outputs radar reflectivity. To bridge this gap, we compute a cloud mask from the simulated radar reflectivity using a threshold of  $-20 \text{ dBZ}$  to discriminate cloudy and clear air. This threshold is arbitrary, but the main conclusions are the same if a threshold of  $-25$  or  $-10 \text{ dBZ}$  is used instead. Simulated CloudSat and CALIPSO data are then combined to produce a cloud mask derived from both sensors. Since the cloud retrieval algorithm differs between the observations and the model, these data should be compared qualitatively only. However, a qualitative comparison is still useful, since it can reveal the shortcomings of the model.

We also examine several other aspects of the simulated clouds. First, we compare the observed and simulated clouds using a MODIS simulator, which allows for a direct model-to-observation comparison. We also examine the cloud fraction profile that is output directly from the model, without being passed through a satellite simulator. These steps are taken to ensure that our simple CloudSat retrieval algorithm does not misrepresent the clouds simulated by CAM5.

Finally, note that the model simulations and observations come from the same decade but only partially overlap, so interannual variations could contribute to differences between CAM5 and the observations. To check this, we examined the cloud-circulation relationships computed from each individual year. Year-to-year differences in CAM5 and year-to-year differences in the observations are small compared to the difference between CAM5 and the observations (Figure S3). Therefore, the differences in observed and simulated clouds shown herein reflect biases in CAM5.

### 3. Results

#### 3.1. Cloud-Circulation Relationships Deduced From Satellite Observations

Our goal is to study the relationship between clouds and large-scale circulations. We consider circulations to be large-scale if they are broad enough to be resolved in the reanalysis data. This includes circulations with length scales of at least 200 km and time scales of at least 6–12 hr (Figure S7). These minimum scales are

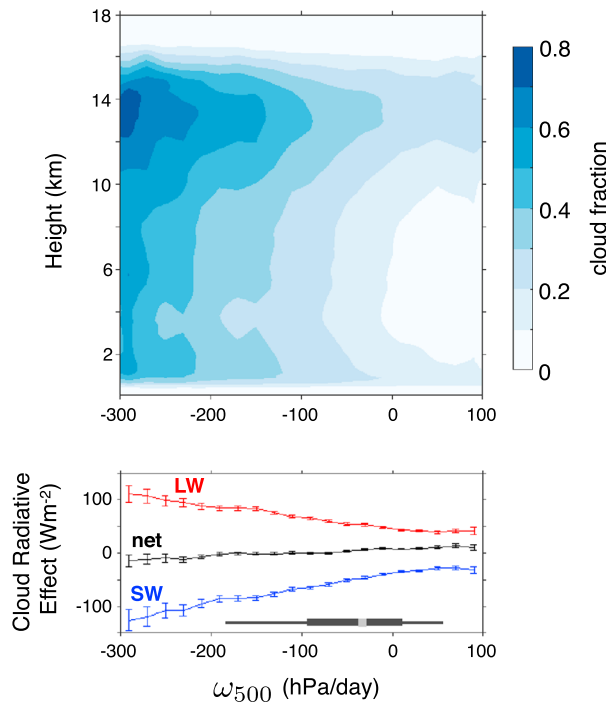


**Figure 1.** The observed relationship between clouds and large-scale vertical motion over the tropical West Pacific. (top) Cloud vertical structure and (bottom) cloud radiative effects. The error bars show the 95% confidence interval for the mean. The box plots show the 5th, 25th, 50th, 75th, and 95th percentiles of  $\omega_{500}$ .

comparable to the lifetime and size of individual mesoscale convective systems (Igel et al., 2014; Roca et al., 2017). Hence, in the analysis that follows, the cloud properties represent averages over entire convective systems, or nearly so.

Observed cloud-circulation relationships are shown in Figure 1. A distinct peak in cloudiness is observed around 14 km corresponding to anvil cloud detrained from deep convection. From 8 to 5 km, clouds are observed with a similar frequency at all levels, as indicated by the vertical contours. A slight local maximum in cloud cover is seen near the surface corresponding to trade cumulus. As large-scale upward motion increases, cloud cover increases, but the vertical profile of cloudiness remains remarkably similar. This symmetry of the cloud population is reflected in CRE: As upward motion increases, SW and LW CRE both increase in magnitude, but they do so at nearly equal and opposite rates. Thus, the net CRE remains nearly neutral across a wide range of large-scale vertical motions. A similar relationship is seen when the cloud fields are binned by low-level divergence from scatterometer observations, lending credibility to this result (Figure S1).

The distribution of CREs is shown in Figure 2. In this figure the observations are separated into three composites based on the terciles of  $\omega_{500}$ , including strong ascent ( $\omega_{500} \leq -71 \text{ hPa d}^{-1}$ ), weak ascent ( $-71 < \omega_{500} \leq -2 \text{ hPa d}^{-1}$ ), and subsidence ( $\omega_{500} > -2 \text{ hPa d}^{-1}$ ). The subsidence regime mostly consists of albedo below 0.3 and OLR above  $150 \text{ Wm}^{-2}$ . In the weak ascent regime, thick and intermediate anvil clouds with higher albedo and lower OLR are observed as well, and these cloud types are even more common in the strong ascent regime. The average top-of-atmosphere flux of net radiation ( $R_{\text{net}}$ ) for the strong ascent, weak ascent, and subsidence regimes are  $80.7$ ,  $86.5$ , and  $86.4 \text{ Wm}^{-2}$ , respectively.

However, a large spread about these mean values is observed due to the diversity of cloud types produced by convection. Deviations from the mean  $R_{\text{net}}$  range from  $-94 \text{ Wm}^{-2}$  (first percentile) to  $+65 \text{ Wm}^{-2}$  (99th percentile). The bottom row of Figure 2 shows the relative contribution of various albedo-OLR pairings to the radiation budget, which indicates the cloud types that contribute to the CRE balance. In the strong ascent regime, net cooling effects from the brightest clouds, which have albedo around 0.7 and OLR around  $120 \text{ Wm}^{-2}$ , balance net warming effects from clouds with albedo below 0.3 and OLR between 150 and  $280 \text{ Wm}^{-2}$ . In the subsidence regime the majority of the radiation balance is between clouds with albedo below 0.2 and OLR between 200 and  $300 \text{ Wm}^{-2}$ , and in the weak ascent regime, all of the aforementioned cloud types contribute to the radiation balance. These findings indicate that deep-convective systems produce a diverse ensemble of clouds, but the cloud ensemble tends to have an aggregate radiative effect that is similar to the background, nonconvective environment. Thus, stronger large-scale ascent increases high-cloud cover but has a weak effect on the flux of net radiation at the top of the atmosphere.

### 3.2. Cloud-Circulation Relationships in CAM5

Next we examine relationships between clouds and large-scale circulation in CAM5. This evaluation applies to a simulation with SSTs prescribed to observed values, so the impacts of cloud-SST interactions cannot be addressed here. However, the purpose of this section is to describe the general features of deep-convective clouds simulated by a CMIP5 model. For this purpose, simulations with prescribed SSTs are sufficient.

Figures 3a and 3b show the vertical structure of cloud fraction in observations and the vertical structure of hydrometeor fraction simulated by CAM5. Both are derived from CloudSat and CALIPSO data, but different retrieval algorithms are used. These quantities must therefore be compared qualitatively (section 2.3). The vertical structure of observed and simulated clouds is quite different. Observed convective clouds have a peak in high cloudiness associated with anvil clouds, while the simulated convective clouds are wide and towering, and lack a distinct upper-level peak. The cloud profile output directly from CAM5, without the use of a satellite simulator, shows a similar result (Figures S4 and S5).

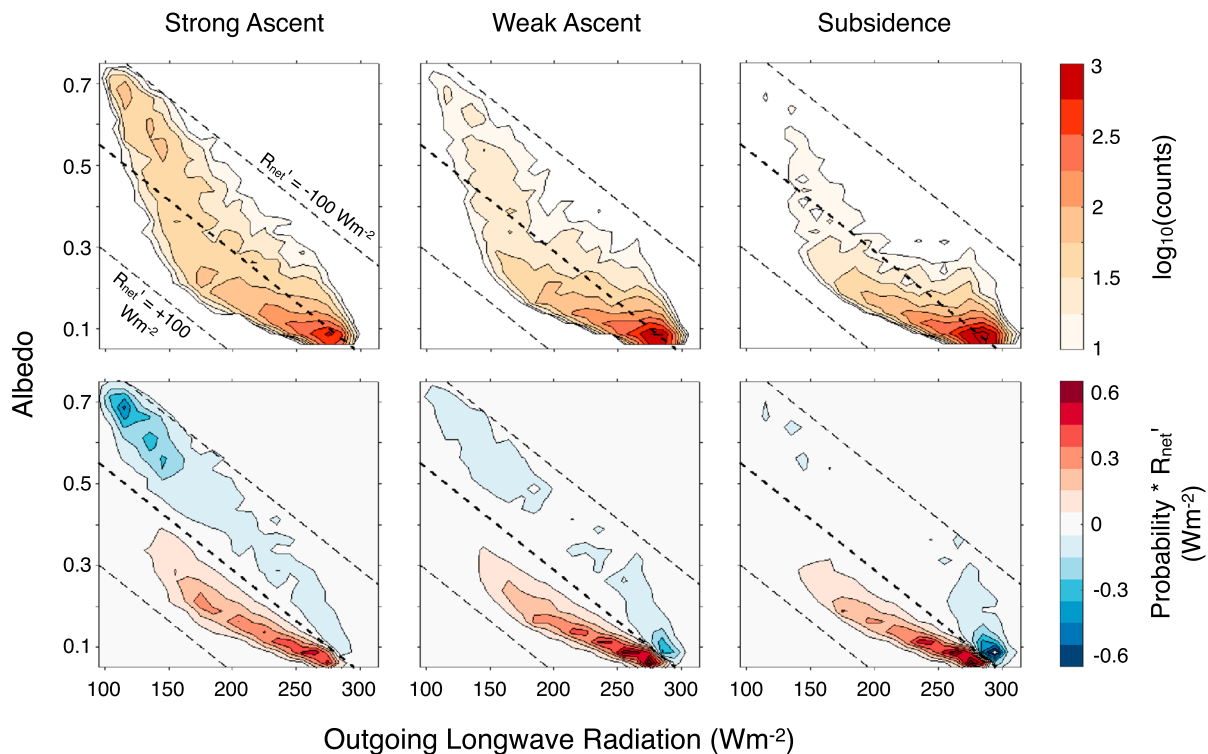


**Figure 2.** The observed distribution of albedo and outgoing longwave radiation (OLR) as a function of large-scale vertical motion. (top row) Joint histograms of albedo and OLR separated into conditions of strong ascent, weak ascent, and subsidence based on the terciles of  $\omega_{500}$ . The dashed lines show albedo-OLR pairings that correspond to differences of  $-100, 0,$  and  $+100 \text{ Wm}^{-2}$  from the domain-average top-of-atmosphere net radiation ( $R_{\text{net}}$ ). (bottom row) Probability of each bin multiplied by the  $R_{\text{net}}$  contrast relative to the mean. This indicates the relative contribution of various albedo-OLR pairings to the top-of-atmosphere radiation budget. Bin widths are  $0.025$  for albedo and  $10 \text{ Wm}^{-2}$  for OLR. Average  $R_{\text{net}}$  values for the strong ascent, weak ascent, and subsidence composites are  $80.7, 86.5,$  and  $86.4 \text{ Wm}^{-2}$ , respectively.

The properties of high clouds, which are defined as clouds with tops above 440 hPa in CAM5 and above 7 km in the observations, are described further in Figures 3c–3e. These panels show MODIS data, so CAM5 output and observational data can be compared directly here. High clouds are stratified by optical depth ( $\tau$ ), including optically thick ( $\tau > 23$ ), medium ( $3.6 < \tau \leq 23$ ), and thin ( $1.3 < \tau \leq 3.6$ ) clouds. Thin cirrus clouds with optical depths below 1.3 are common in the tropics (Haladay & Stephens, 2009), but they are excluded here to avoid artifacts in the MODIS observations (Pincus et al., 2012). CAM5 overestimates the coverage of thick high clouds and slightly underestimates the coverage of thin cirrus, and for all but the strongest updrafts, CAM5 also overestimates the coverage of high clouds with medium optical depth. The largest biases are associated with thick clouds, and these biases increase with stronger upward motion. This is further evidence that CAM5 overestimates the proportion of deep clouds and underestimates the proportion of medium-to-thin anvils.

The implications of these biases for the radiation budget are shown in Figures 3f–3h. The simulated convective clouds are too bright and reflect tens of watts per square meter more SW radiation than the observed clouds. Biases in LW CRE are substantially smaller, probably because the tops of the simulated convective clouds are located near the correct altitude (Figures 3a and 3b). Since the SW biases outpace the LW biases, the simulated convective clouds have a negative bias in net CRE that increases in magnitude with stronger ascent (Figure 3h). The root of this bias is a lack of clouds with albedo between 0.1 and 0.3 and OLR between 150 and 250  $\text{Wm}^{-2}$ , which are typical values for medium-to-thin anvils (Figure S6).

Finally, note that the simulated and observed  $\omega_{500}$  distributions are similar (Figure 3i). Cloud biases in CAM5 are therefore likely due to shortcomings of the cloud parameterizations, rather than biases in large-scale circulation, as expected.

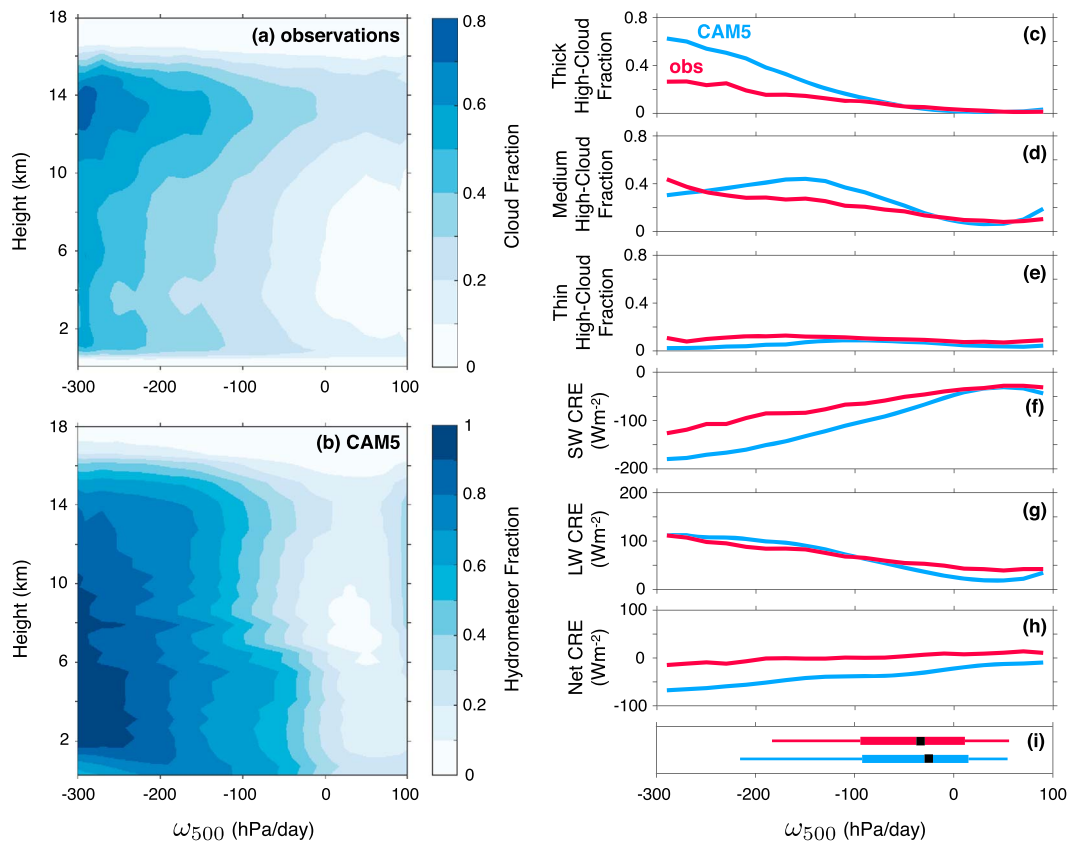


**Figure 3.** Relationships between cloud properties and large-scale vertical motion in observations and CAM5. Vertical profiles of (a) observed cloud fraction and (b) simulated hydrometeor fraction. Both are derived from CloudSat and CALIPSO data but are computed from different retrieval algorithms, so they should be compared qualitatively (see text). (c–e) The fraction of optically thick, medium, and thin high-clouds from MODIS data and (f–h) cloud radiative effects. The box plots in (i) show the 5th, 25th, 50th, 75th, and 95th percentiles of  $\omega_{500}$ . In (c)–(i), the observations and model output can be compared quantitatively.

## 4. Discussion

### 4.1. Evaluating the Hypotheses for the CRE Balance

Hartmann et al. (2001) were the first to argue that the CRE balance may not be coincidental. They hypothesized that feedbacks between cloud albedo, large-scale circulation, and SST could constrain the top-of-atmosphere net radiation to be uniform in the warm tropics, thus constraining the net CRE to be small. They developed a toy model to illustrate this concept. The model includes a warm region of active convection, a cooler region of suppressed convection, and a large-scale overturning cell that connects them. All of the model components interact through negative feedbacks. For instance, if SSTs warm in the convective region, then the enhanced SST gradient between the convective and non-convective regions strengthens the overturning cell, which enhances convection and albedo in the convective region. The additional shading of the ocean surface reduces the SST perturbation and ultimately returns the system to equilibrium. If these self-regulating feedbacks are sufficiently strong, then they limit SST gradients to small values, and with only weak temperature gradients to act on, the large-scale overturning circulations become relatively inefficient in transporting energy horizontally. To conserve energy, the top-of-atmosphere net radiation in the convective region is constrained to be close to that in the neighboring nonconvective region.

Two statements from Hartmann et al.'s (2001) argument can be tested here. First, their model *assumes* that cloud albedo increases linearly with stronger upward motion, if both are averaged over scales larger than individual storms. We find this assumption to be justified, despite previous criticism (Figure 1; Chou & Lindzen, 2002). Second, their model *predicts* that the top-of-atmosphere net radiation will be very close in neighboring convective and nonconvective regions. We find this to be true as well. The average top-of-

atmosphere net radiation in regions of strong upward motion differs by only  $6 \text{ Wm}^{-2}$  from that in regions of subsidence (Figure 2).

A second hypothesis for the CRE balance was recently proposed by Hartmann and Berry (2017). They noted that radiative balance over the west Pacific warm pool results from a cancellation between thick anvil clouds, which are less common but have a strong cooling effect, and associated thin cirrus clouds, which are much more common but have a weaker warming effect. Radiative neutrality is thus a feature of the lifecycle of individual convective cloud complexes in the tropics. They then investigated the impact of cloud radiative heating on overhanging anvil clouds. LW absorption preferentially occurs near cloud base, so it destabilizes the cloud layer and encourages in-cloud turbulent mixing. The turbulent updrafts within the upper-level ice cloud could promote fresh nucleation of ice crystals near the cloud boundary and thereby extend the lifetime of the cloud. Since these effects are stronger in medium-to-thin anvils than in deep clouds, Hartmann and Berry (2017) hypothesized that cloud radiative heating could explain the relative abundance of thin cirrus and hence could be central to explaining the CRE balance.

If Hartmann and Berry's (2017) hypothesis is correct, then large-scale circulations can promote or discourage convection, but ultimately, the cloud population is driven toward a neutral radiative effect by processes that operate on the scale of individual convective systems, making the net CRE less sensitive to the large-scale flow. If this is true, then CRE will remain balanced as circulation varies. The weak sensitivity of net radiation to variations in large-scale circulation is therefore consistent with Hartmann and Berry's (2017) hypothesis.

Of course it is possible that both the Hartmann et al. (2001) and the Hartmann and Berry (2017) mechanisms are important. The sensitivity of net radiation and net CRE to vertical motion is weak (Figure 1, bottom), which must be the result of tropical cloud systems including an amount of thin high cloud in proportion to the amount of deep convection and precipitation, as Hartmann and Berry (2017) suggested, and as is indicated by the top panel of Figure 1. The net CRE does trend slightly negative with increasing upward motion, however, which could help with the mechanism proposed by Hartmann et al. (2001), in which the radiative effect of deep convection in cooling the surface and warming the atmosphere is a constraint on the net CRE.

#### 4.2. Implications for Climate Projections

Suppose that the CRE balance is not coincidental but is maintained by some robust process internal to the climate system. Furthermore, imagine a climate model that lacks this process. The model can be tuned to have balanced CRE in the current climate, but if it lacks the process that causes the CRE balance, then the model may simulate erroneous cloud feedbacks in response to changes in climate. Such errors could have far-reaching impacts on climate projections because deep convection fundamentally shapes tropical temperatures and circulation (Hartmann et al., 1984). Thus, if the radiative balance in the convective tropics is strongly modulated by some robust process, then it is crucial that climate models are able to simulate that process with fidelity.

It is therefore important to ask if climate models are capable of simulating the mechanisms that have been proposed to explain the CRE balance. First, consider the hypothesis that the CRE balance is caused by interactions between cloud albedo, large-scale circulation, and SST (Hartmann et al., 2001). At its core, this hypothesis relies on large-scale energy and mass conservation—both of which are respected by climate models. Furthermore, the hypothesis makes predictions about the interactions between clouds, circulation, and SST on scales broad enough to be resolved by current GCMs. If this hypothesis is realistic, then it may apply to current GCMs with standard resolution.

Alternatively, consider the possibility that the CRE balance is caused by interactions between cloud radiative heating, convective turbulence, and cloud microphysics within extended anvil clouds (Hartmann & Berry, 2017). We find that the proportion of deep and optically thick cloud is far too large in CAM5, and the proportion of medium-to-thin anvil is too small. This suggests that extended anvil clouds are not well represented in CAM5, perhaps because radiation-turbulence-microphysics interactions in anvil clouds are poorly represented. If these interactions fundamentally control the proportion of optically thick and thin high-clouds in the tropics, then it may be necessary to improve the parameterization of these processes, or to explicitly resolve them, to accurately simulate future climate change.

## 5. Conclusion

A long-standing open problem in climate research is to explain why the average SW and LW CRE are nearly equal and opposite over the warm and convective tropical oceans. In this study we demonstrate that the radiative balance in the tropics is maintained across a wide range of large-scale circulations, as long as CREs are averaged over scales that are larger than individual storms. Stronger upward motion is associated with enhanced deep-convection, but the proportion of thick, medium, and thin anvil cloud remains approximately constant as vertical motion varies. As a result, the SW and LW CRE both increase in magnitude with stronger ascent, but they do so at nearly equal and opposite rates (Figure 1). The top-of-atmosphere net radiation is therefore only weakly sensitive to large-scale vertical motion. For instance, the top-of-atmosphere net radiation in regions of strong upward motion differs from that in regions of subsidence by only  $6 \text{ Wm}^{-2}$  (Figure 2).

Furthermore, we ask if the CAM5 reproduces the observed cloud-circulation relationships. The population of deep-convective clouds in CAM5 differs substantially from the observations. Most notably, CAM5 overestimates the proportion of deep and optically thick cloud and underestimates the proportion of medium-to-thin anvil. Thus, simulating the structure and optical properties of deep-convective clouds remains challenging for at least some CMIP5 models.

These results highlight the importance of determining if the tropical CRE balance is coincidental, and if it is not, then determining the scale of the process responsible for maintaining the balance. If the process is large enough in scale to be resolved by current GCMs, as hypothesized by Hartmann et al. (2001), then GCMs may be capable of adequately simulating it, despite the challenges associated with simulating the details of individual convective systems. If the process is small in scale, like the radiation-turbulence-microphysics interactions proposed by Hartmann and Berry (2017), then it may be necessary to devote resources toward high-resolution global modeling or to develop parameterizations that can mimic the physics in extended stratiform anvil clouds. Given the computational challenges associated with direct simulation of anvil cloud physics, and the intellectual challenges associated with developing a suitable parameterization, it is important to determine which scenario is correct and to direct our efforts accordingly.

## Acknowledgments

This work was supported by the Regional and Global Climate Modeling Program of the Office of Science of the U.S. Department of Energy (grant DE-SC0012580). We gratefully acknowledge Trude Storelvmo for insightful discussion that improved this study, Jen Kay for guidance on running the satellite simulator software, and two anonymous reviewers for their helpful comments. We would like to acknowledge high-performance computing support from Cheyenne (doi:10.5065/D6RX99HX) provided by NCAR's Computational and Information Systems Laboratory, sponsored by the National Science Foundation. The A-Train satellite data used in this study are available from <https://ceres.larc.nasa.gov/>, the ECMWF reanalysis data are available from <http://apps.ecmwf.int/datasets/>, the QuikSCAT scatterometer data are available from <https://podaac.jpl.nasa.gov/>, and the CAM5 data are available from <ftp://eos.atmos.washington.edu/pub/caseyw8>.

## References

- Bodas-Salcedo, A., Webb, M. J., Bony, S., Chepfer, H., Dufresne, J.-L., Klein, S. A., et al. (2011). COSP: Satellite simulation software for model assessment. *Bulletin of the American Meteorological Society*, 92(8), 1023–1043. <https://doi.org/10.1175/2011BAMS2856.1>
- Bretherton, C. S., & Hartmann, D. L. (2009). Large-scale controls on cloudiness. In *Peer-reviewed book chapter for perturbed clouds in the climate system: Their relationship to energy balance, atmospheric dynamics and precipitation Strungmann forum reports* (Vol. 2, pp. 217–234). Cambridge, MA: MIT Press. <https://doi.org/10.7551/mitpress/9780262012874.003.0010>
- Bretherton, C. S., & Park, S. (2009). A new moist turbulence parameterization in the Community Atmosphere Model. *Journal of Climate*, 22(12), 3422–3448. <https://doi.org/10.1175/2008JCLI2556.1>
- Caldwell, P. M., Zelinka, M. D., Taylor, K. E., & Marvel, K. (2016). Quantifying the sources of intermodel spread in equilibrium climate sensitivity. *Journal of Climate*, 29(2), 513–524. <https://doi.org/10.1175/jcli-d-15-0352.1>
- CERES Science Team (2016). CERES CCCM, version ReIB1. Subset: July 2006–August 2010, accessed 22 July 2016. Retrieved from <https://ceres.larc.nasa.gov/products.php?product=CCCM>
- CERES Science Team (2017a). CERES\_SYN1deg\_Ed4A data quality summary (10/3/2017). Retrieved from [https://ceres.larc.nasa.gov/documents/DQ\\_summaries/CERES\\_SYN1deg\\_Ed4A\\_DQS.pdf](https://ceres.larc.nasa.gov/documents/DQ_summaries/CERES_SYN1deg_Ed4A_DQS.pdf)
- CERES Science Team (2017b). CERES SYN1deg-1Hour, edition 4A. Subset: June 2008 – August 2008, accessed 1 May 2018. Retrieved from <https://ceres.larc.nasa.gov/products.php?product=SYN1deg>
- Chepfer, H., Bony, S., Winker, D., Chiriaco, M., Dufresne, J.-L., & Sèze, G. (2008). Use of CALIPSO lidar observations to evaluate the cloudiness simulated by a climate model. *Geophysical Research Letters*, 35, L15704. <https://doi.org/10.1029/2008GL034207>
- Chou, M. D., & Lindzen, R. S. (2002). Comments on "Tropical convection and the energy balance at the top of the atmosphere". *Journal of Climate*, 15(17), 2566–2570. [https://doi.org/10.1175/1520-0442\(2002\)015<2566:COTCAT>2.0.CO;2](https://doi.org/10.1175/1520-0442(2002)015<2566:COTCAT>2.0.CO;2)
- Dee, D. P., Uppala, S. M., Simmons, A. J., Berrisford, P., Poli, P., Kobayashi, S., et al. (2011). The ERA-Interim reanalysis: Configuration and performance of the data assimilation system. *Quarterly Journal of the Royal Meteorological Society*, 137(656), 553–597. <https://doi.org/10.1002/qj.828>
- Dufresne, J.-L., & Bony, S. (2008). An assessment of the primary sources of spread of global warming estimates from coupled atmosphere-ocean models. *Journal of Climate*, 21(19), 5135–5144. <https://doi.org/10.1175/2008JCLI2239.1>
- ECMWF (2015). ERA-Interim project. Subset: 6-hourly, July 2006–August 2010. Accessed 22 July, 2016. Retrieved from <http://apps.ecmwf.int/datasets/>
- Fore, A. G., Stiles, B. W., Chau, A. H., Williams, B. A., Dunbar, R. S., & Rodriguez, E. (2014). Point-wise wind retrieval and ambiguity removal improvements for the QuikSCAT climatological data set. *IEEE Transactions on Geoscience and Remote Sensing*, 52(1), 51–59. <https://doi.org/10.1109/TGRS.2012.2235843>
- Gates, W. L. (1992). AMIP: The Atmospheric Model Intercomparison Project. *Bulletin of the American Meteorological Society*, 73(12), 1962–1970. [https://doi.org/10.1175/1520-0477\(1992\)073<1962:ATAMIP>2.0.CO;2](https://doi.org/10.1175/1520-0477(1992)073<1962:ATAMIP>2.0.CO;2)

- Haladay, T., & Stephens, G. (2009). Characteristics of tropical thin cirrus clouds deduced from joint CloudSat and CALIPSO observations. *Journal of Geophysical Research*, 114, D00A25. <https://doi.org/10.1029/2008JD010675>
- Hartmann, D. L., & Berry, S. E. (2017). The balanced radiative effect of tropical anvil clouds. *Journal of Geophysical Research: Atmospheres*, 122, 5003–5020. <https://doi.org/10.1002/2017JD026460>
- Hartmann, D. L., Hendon, H. H., & Houze, R. A. (1984). Some implications of the mesoscale circulations in tropical cloud clusters for large-scale dynamics and climate. *Journal of the Atmospheric Sciences*, 41(1), 113–121. [https://doi.org/10.1175/1520-0469\(1984\)041<0113:SIOTMC>2.0.CO;2](https://doi.org/10.1175/1520-0469(1984)041<0113:SIOTMC>2.0.CO;2)
- Hartmann, D. L., Moy, L. A., & Fu, Q. (2001). Tropical convection and the energy balance at the top of the atmosphere. *Journal of Climate*, 14(24), 4495–4511. [https://doi.org/10.1175/1520-0442\(2001\)014<4495:TCATEB>2.0.CO;2](https://doi.org/10.1175/1520-0442(2001)014<4495:TCATEB>2.0.CO;2)
- Haynes, J. M., Marchand, R. T., Luo, Z., Bodas-Salcedo, A., & Stephens, G. L. (2007). A multipurpose radar simulation package: Quickbeam. *Bulletin of the American Meteorological Society*, 88(11), 1723–1728. <https://doi.org/10.1175/BAMS-88-11-1723>
- Igel, M. R., Drager, A. J., & van den Heever, S. C. (2014). A CloudSat cloud object partitioning technique and assessment and integration of deep convective anvil sensitivities to sea surface temperature. *Journal of Geophysical Research: Atmospheres*, 119, 10,515–10,535. <https://doi.org/10.1002/2014JD021717>
- Kato, S., Miller, W. F., Sun-Mack, S., Rose, F. G., & Chen, F. (2010). Variable descriptions of the A-Train integrated CALIPSO, CloudSat, CERES, and MODIS merged product (CCC or C3M). Retrieved from [https://eosweb.larc.nasa.gov/project/ceres/readme/c3m\\_variables\\_B1\\_v2.pdf](https://eosweb.larc.nasa.gov/project/ceres/readme/c3m_variables_B1_v2.pdf)
- Kiehl, J. T. (1994). On the observed near cancellation between longwave and shortwave cloud forcing in tropical regions. *Journal of Climate*, 7(4), 559–565. [https://doi.org/10.1175/1520-0442\(1994\)007<0559:OTONCB>2.0.CO;2](https://doi.org/10.1175/1520-0442(1994)007<0559:OTONCB>2.0.CO;2)
- Klein, S. A., & Jakob, C. (1999). Validation and sensitivities of frontal clouds simulated by the ECMWF model. *Monthly Weather Review*, 127(10), 2514–2531. [https://doi.org/10.1175/1520-0493\(1999\)127,2514:VASOFC.2.0.CO;2](https://doi.org/10.1175/1520-0493(1999)127,2514:VASOFC.2.0.CO;2)
- Morrison, H., & Gettelman, A. (2008). A new two-moment bulk stratiform cloud microphysics scheme in the Community Atmosphere Model, version 3 (CAM3). Part I: Description and numerical tests. *Journal of Climate*, 21(15), 3642–3659. <https://doi.org/10.1175/2008JCLI2105.1>
- Neale, R. B., Chen, C.-C., Gettelman, A., Lauritzen, P. H., Park, S., Williamson, D. L., et al. (2012). Description of the NCAR Community Atmosphere Model (CAM5). National Center for Atmospheric Research Technical Note. NCAR/TN-486+STR. Retrieved from [http://www.cesm.ucar.edu/models/cesm1.0/cam/docs/description/cam5\\_desc.pdf](http://www.cesm.ucar.edu/models/cesm1.0/cam/docs/description/cam5_desc.pdf)
- Park, S., & Bretherton, C. S. (2009). The University of Washington shallow convection and moist turbulence schemes and their impact on climate simulations with the Community Atmosphere Model. *Journal of Climate*, 22(12), 3449–3469. <https://doi.org/10.1175/2008JCLI2557.1>
- Park, S., Bretherton, C. S., & Rasch, P. J. (2014). Integrating cloud processes in the Community Atmosphere Model, version 5. *Journal of Climate*, 27(18), 6821–6856. <https://doi.org/10.1175/JCLI-D-14-00087.1>
- Pincus, R., Platnick, S., Ackerman, S. a., Hemler, R. S., & Patrick Hofmann, R. J. (2012). Reconciling simulated and observed views of clouds: MODIS, ISCCP, and the limits of instrument simulators. *Journal of Climate*, 25(13), 4699–4720. <https://doi.org/10.1175/JCLI-D-11-00267.1>
- Ramanathan, V., Cess, R. D., Harrison, E. F., Minnis, P., Barkstrom, B. R., Ahmad, E., et al. (1989). Cloud-radiative forcing and climate: Results from the Earth radiation budget experiment. *Science*, 243(4887), 57–63. <https://doi.org/10.1126/science.243.4887.57>
- Roca, R., Fiolleau, T., & Bouniol, D. (2017). A simple model of the life cycle of mesoscale convective systems cloud shield in the tropics. *Journal of Climate*, 30, 4283–4298. <https://doi.org/10.1175/JCLI-D-16-0556.1>
- Sassen, K., & Wang, Z. (2008). Classifying clouds around the globe with the CloudSat radar: 1-year of results. *Geophysical Research Letters*, 35, L04805. <https://doi.org/10.1029/2007GL032591>
- SeaPAC (2018). QuikSCAT level 2B ocean wind vectors in 12.5km slice composites version 4.0. PO.DAAC, CA, USA. Subset July 2006 – August 2009, accessed 1 May 2018. Retrieved from <https://doi.org/10.5067/QSX12-L2B01>
- Stephens, G. L., Vane, D. G., Boain, R. J., Mace, G. G., Sassen, K., Wang, Z., et al., & the CloudSat Science Team (2002). The CloudSat mission and the A-Train. *Bulletin of the American Meteorological Society*, 83(12), 1771–1790. <https://doi.org/10.1175/BAMS-83-12-1771>
- Zhang, G. J., & McFarlane, N. A. (1995). Sensitivity of climate simulations to the parameterization of cumulus convection in the Canadian Climate Centre general circulation model. *Atmosphere-Ocean*, 33(3), 407–446. <https://doi.org/10.1080/07055900.1995.9649539>